Journal of Sound and Vibration (2000) **000**(0), 000–000
doi:10.1006/jsvi.2000.2963, available online at http://www.idealibrary.com on IDEAL®

THE *xyzr* ALGORITHM SPECIALIZED FOR EIGENVIBRATION PROBLEM OF BORED AND LAMINATED OBJECTS

AKIRA YONEDA

Institute for Study of the Earth's Interior, Okayama University, Misasa, Tottori 682-0193, *Japan*

(*Received* 27 *July* 1999, *and in final form* 8 *February* 2000)

We can determine elastic properties of an object from its eigenvibration frequencies, as long as a numerical calculation algorithm is available for the eigenvibration frequencies. The *xyz* algorithm developed by Visscher *et al.* [1] is an extremely versatile method applicable even for anisotropic, inhomogeneous, and irregular-shaped objects, with the exception of bored and laminated systems. I examined the characteristics and performance of the original *xyz* algorithm, and succeeded in developing the *xyzr* algorithm for bored and laminated sphere and cylinder. The accuracy and convergency of the *xyzr* algorithm are examined by comparison with analytical solutions; the method is accurate enough for us to develop a new experimental technique to obtain the elastic properties of soft materials accommodated in a solid container.

1. INTRODUCTION

The eigenvibration problem has been analyzed by means of the Rayleigh–Ritz method based on Hamilton's principle. Holland [2] solved the eigenvibration problem for a cube with cubic crystallographic symmetry by using trigonometric functions as the base functions. Demarest [3] improved convergence of the same problem by introducing Legendre polynomials as base functions. Ohno [4] expanded Demarest's solution to a parallelepiped rectangle with orthorhombic crystallographic symmetry. Senoo and Nishimura [5] obtained a numerical solution for a cylinder by combining the Rayleigh–Ritz method and the finite element method by using Legendre polynomials for base functions as well. However, further progress has not yet been achieved in this analyzing scheme owing to difficulty in manipulating Legendre polynomials.

The *xyz* algorithm by Visscher *et al.* [1] provided a breakthrough in this field. They showed that simple power functions in Cartesian co-ordinates can be used for the base functions (Appendix A). The *xyz* algorithm enables an easy analysis of eigenvibration, even for objects with internal inhomogenenity, elastic anisotropy, and irregular shape.

The versatility of the *xyz* algorithm inspired me to devise a new experimental technique to investigate the rheological properties of liquid and soft materials by measuring eigenvibration frequencies of a container filled with the target material. However, I found that the *xyz* algorithm is not so accurate for an object with inner and outer interfaces such as a spherical shell or tube (see section 3).

Through examining the characteristics of the *xyz* algorithm, I developed the *xyzr* algorithm as a solution for a spherical shell or a tube. Here, I discuss first the characteristics

0022-460X/00/000000 + 00 $35.00/0

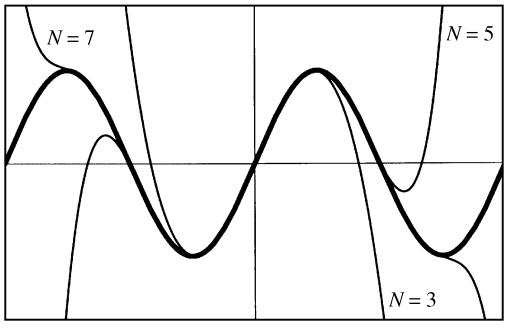

Figure 1. An example showing how a sinusoidal function is fitted well by power functions. Note that odd powers $\{x, x^3, x^5, x^7\}$ were used in the fitting because the sine function (thick line) is an odd function. Thin lines are the resultant polynomial functions after fitting; N is the maximum power used in the fitting. For instance, $N = 5$ specifies that the set of $\{x, x^3, x^5\}$ are used in the fitting. We can see that the fittable range increases with increasing N.

of the *xyz* algorithm by comparison with analytical solutions, and then introduce the *xyzr* algorithm and show its performance.

In the following discussion, please note the differences among solid, bored, and laminated objects with spherical or cylindrical symmetry. Namely, solid sphere and cylinder do not have an empty region inside, whereas, bored objects are identical with a shell and a tube and are empty inside. Laminated objects are two layered without an empty region inside.

2. CHARACTERISTICS OF THE *xyz* METHOD

It is quite curious why the *xyz* method works so widely and accurately in various eigenvibration problems. A displacement function for standing waves, $u_i(x, y, z)$, is generally given

$$u_i(x, y, z) = e^{i\omega t} \sin(lx + p_x) \sin(my + p_y) \sin(nz + p_z)\, \mathbf{e}_i, \tag{1}$$

where ω is the angular frequency, and $\mathbf{e}_i$ a directional unit vector in the ith direction ($i = 1, 2, 3$) in the Cartesian co-ordinate. Any eigenvibration mode can be expressed as a superposition of the above equations. Fundamental modes of eigenvibration are specified by wave numbers standing in a vibrating body, or numbers of nodal surfaces. Figure 1 shows how finite power functions approximate well a sinusoidal function, or a standing wave excited in a body. We can judge that a mode of $w_n = 0{\cdot}5$ (w_n: wave number over sample dimension) may be calculated accurately even at $N = 3$; identically, for $w_n = 1{\cdot}0$, at $N = 5$ and for $w_n = 1{\cdot}5$, at $N = 7$ respectively. A simplified relation is that N is required to be 5–6 times that of w_n.

I confirmed the above discussion by examining eigenvibrations for an isotropic sphere, whose eigenvibration modes can be calculated analytically. In the following discussion, please note that physical properties of an object are always fixed at $\sigma = 0{\cdot}25$ (σ the Poisson ratio), or $v_p = \sqrt{3} v_s$ (v_p the longitudinal wave velocity; v_s the shear wave velocity), and analytical eigenfrequencies are always normalized by v_s/d_0 (d_0 the diameter of sphere or cylinder).

In spherical co-ordinates, the analytical solutions of displacement are expressed as a product of the spherical Bessel function, j ($j_n(x) = \mathrm{J}_n(x)/x^{1/2}$; J being the first kind of Bessel

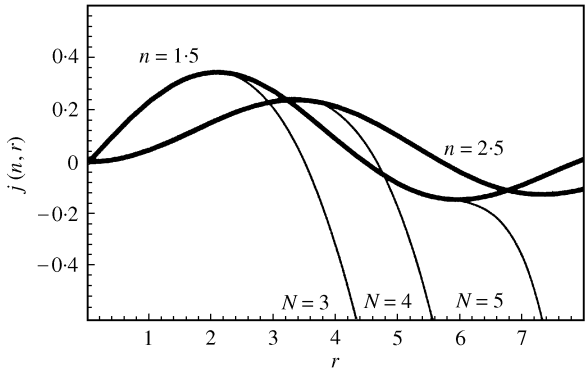

Figure 2. An example showing how the first kind of spherical Bessel function is fitted well by power functions. Thick lines are $j_{1\cdot5}(r)$ and $j_{2\cdot5}(r)$, in the displacement functions of ${}_qS_0$ and ${}_0T_n$ respectively. Procedures are similar to that in Figure 1. Note that $N = 3$, 4, and 5 specify the set of power functions used, or $\{r^1, r^3\}$, $\{r^0, r^2, r^4\}$, and $\{r^1, r^3, r^5\}$ respectively.

function), the Legendre polynomial function, P, and the trigonometric functions. Displacement functions of some fundamental modes are as follows (Appendix B)

$$ {}_aS_0: \quad U_r = -\frac{h\mathrm{J}_{1\cdot5}(hr)}{\sqrt{r}}, \quad U_\theta = 0, \qquad U_\phi = 0, \tag{2} $$

$$ {}_0T_2: \quad V_r = 0, \qquad V_\theta = 0, $$

$$ V_\phi = \frac{\mathrm{J}_{2\cdot5}(kr)}{\sqrt{r}} \frac{\{(n+1-m)P_{n+1}^m(\cos\theta) - (n+1)\cos\theta P_n^m(\cos\theta)\}}{\sin\theta} \mathrm{e}^{\mathrm{i}m\phi}. \tag{3} $$

The fitness of power functions to the spherical Bessel functions is shown in Figure 2. The first and second extrema of $j_{1\cdot5}(h)$ satisfy the boundary condition of ${}_0S_0$ and ${}_1S_0$ respectively. Therefore, accurate frequencies are expected to be given at $N = 3$ and 5, respectively, for those non-angular modes. This prediction is consistent with the results shown in Table 1. On the other hand, for the ${}_0T_n$ modes, it takes 4° to approximate their radial term. Considering that it requires an additional $n°$ for the angular term, the eigenfrequencies of ${}_0T_2$ and ${}_0T_7$ are expected to be given accurately at $N = 6$ and $N = 11$, respectively, as shown in Table 1. Although only the four modes are demonstrated here, I have checked that the present discussion is exactly valid for other modes.

Before proceeding the numerical evaluation for bored and laminated systems, please note that the inner–outer radius ratio is always fixed at $r_i/r_0 = 0\cdot5$ as a representative case, where the superscripts i and o refer to the inner and outer regions respectively. As shown for the case of $k = 0$ in Table 2, the *xyz* algorithm is not as accurate for a bored sphere, or a spherical shell, as it is for a solid sphere (see Table 1). In this case, a second kind of Bessel function, Y, is introduced in the solutions as explained in Appendix B. In general, y ($= \mathrm{Y}(x)/x^{1/2}$) is hard to be fitted using only positive powers; Figure 3 shows the situation and the necessity of introducing inverse powers to yield better fitting of y. Therefore, I have devised a new algorithm for the bored body as described in the next section.

TABLE 1

Frequencies of the xyz algorithm for some selected modes in a homogeneous isotropic solid sphere. Normalized analytical frequencies are shown in the parentheses below mode indices. The numerical frequencies are normalized by the analytical one of each mode

${}_0S_0$ (1·4133)	$N = 3$: 1·0009 $N = 5$: 1·0000	${}_0T_2$ (0·79614)	$N = 3$: 1·0578 $N = 5$: 1·0002 $N = 7$: 1·0000
${}_1S_0$ (3·3403)	$N = 5$: 1·0007 $N = 7$: 1·0000	${}_1T_1$ (1·8346)	$N = 5$: 1·0160 $N = 7$: 1·0003 $N = 9$: 1·0000
${}_0S_2$ (0.84030)	$N = 3$: 1·0037 $N = 5$: 1·0000	${}_0T_7$ (2·7120)	$N = 9$: 1·0065 $N = 11$: 1·0001 $N = 13$: 1·0000

TABLE 2

Normalized numerical frequencies by the xyz and xyzr algorithms for some selected modes in a bored sphere or a shell with $r_i/r_0 = 0{\cdot}5$. Note that the $k = 0$ corresponds to the xyz algorithm. Normalized analytical frequencies are shown in the parentheses below mode indices

N	k	${}_0S_0$ (1·1228)	${}_0S_2$ (062139)	${}_0T_2$ (0·77520)
7	0	1·0106	1·0194	1·0022
	3	1·0000	1·0105	1·0014
	5	1·0000	1·0037	1·0008
	7	1·0007	1·0197	1·0612
9	0	1·0023	1·0115	1·0009
	3	1·0000	1·0042	1·0001
	5	1·0000	1·0006	1·0001
	7	1·0000	1·0000	1·0004
11	0	1·0004	1·0070	1·0003
	3	1·0000	1·0012	1·0000
	5	1·0000	1·0001	1·0000
	7	1·0000	1·0000	1·0000
13	0	1·0001	1·0032	1·0001
	5	1·0000	1·0003	1·0000
	7	1·0000	1·0000	1·0000
	9	1·0000	1·0000	1·0000
15	0	1·0000	1·0012	1·0000
	5	1·0000	1·0000	1·0000
	7	1·0000	1·0000	1·0000
	9	1·0000	1·0000	1·0000

3. THE *xyzr* ALGORITHM FOR A BORED BODY AND A LAMINATED BODY

Assume a spherical shell with inner and outer radii of r_i and r_0 respectively. I modified base functions as

$$\varphi_\lambda = \frac{x^l y^m z^n}{r^k} \mathbf{e}_i, \tag{4}$$

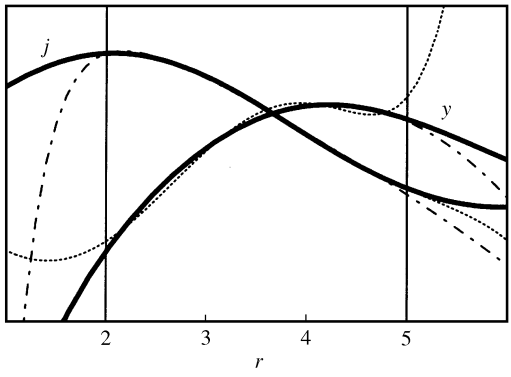

Figure 3. A demonstration showing why inverse powers are required in the fitting of the second kind of spherical Bessel function. Thick lines are $j_{1\cdot5}(r)$ and $y_{1\cdot5}(r)$. The fitted interval is $2 < r < 5$. The dash-dotted lines are the resultant polynomial functions in terms of the set of $\{r^{-3}, r^{-1}, r^1, r^3\}$, while the dotted lines are $\{r, r^3, r^5, r^7\}$. We can see that the set of $\{r, r^3, r^5, r^7\}$ is not suitable to fit $y_{1\cdot5}(r)$ accurately, while the set of $\{r^{-3}, r^{-1}, r^1, r^3\}$ gives reasonable fitting both for j and y functions.

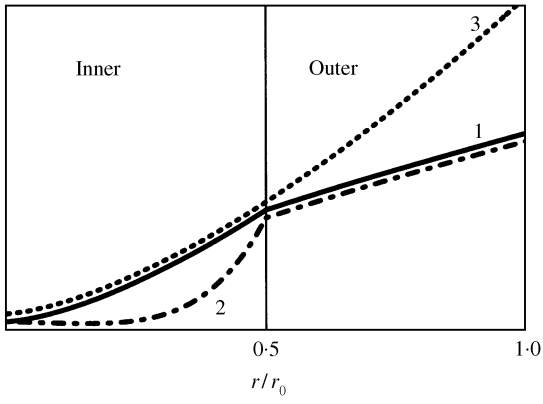

Figure 4. Schematic illustration of various base functions. The numbers correspond to those defined in equations (6)–(8).

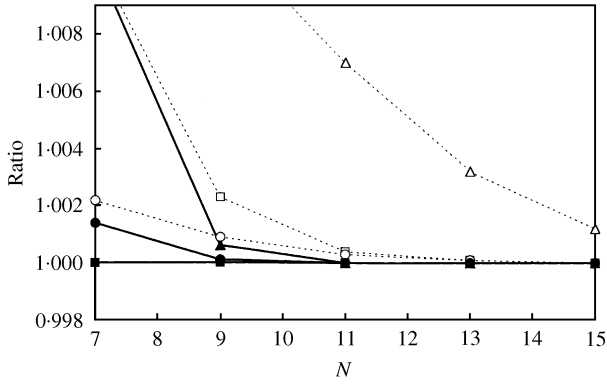

Figure 5. Comparison of convergency between the *xyz* (dotted lines with open symbols) and the *xyzr* (solid lines with solid symbols) algorithms for some selected modes. The data in Table 2 are used. Note that k is chosen to be $\sim N/2$ for the *xyzr* algorithm: - -□- - —■— ${}_0S_0$; - - -△- - - —▲— ${}_0S_2$; - -○- - —●— ${}_0T_2$.

where $r = (x^2 + y^2 + z^2)^{1/2}$ and k is an adjustable parameter to yield the best result. This *xyzr* base function is sufficient for a spherical shell, precluding the co-ordinate origin of $r = 0$. Table 2 shows the accuracy of the *xyzr* algorithm in comparison with that of the *xyz* algorithm for the special case ($k = 0$) of the *xyzr* algorithm. We can recognize a significant improvement using the *xyzr* algorithm. In my experience, the best performance is usually given at $k \sim N/2$; this suggests that the symmetric set of power functions, $\{r^{-k}, r^{-(k-2)}, \ldots, r^{k-2}, r^k\}$, is usually most advantageous for fitting $j(r)$ and $y(r)$ simultaneously. In any case, results are not so sensitive to small variations in k.

The *xyzr* algorithm in cylindrical co-ordinates are the same as those in spherical co-ordinates, except for the definition of r in equation (4). Obviously, $r = (x^2 + y^2)^{1/2}$ is the right choice in the cylindrical co-ordinate; the conversion rule is simply given as

$$r = (x^2 + y^2 + z^2)^{1/2} \to r = (x^2 + y^2)^{1/2}. \tag{5}$$

For a laminated body, we can expect that the *xyz* and the *xyzr* algorithms are useful in the inner and the outer regions respectively. When a laminated sphere is composed of materials with different elastic constants, some derivatives of displacement, or strains, must be discontinuous at the interface, because there the corresponding stresses that are required to be continuous. Thus, we have to prepare base functions in order to be able to adjust for strain discontinuity at the interface. This requirement is satisfied by preparing, at least, two types of base functions. I devised the following three base functions, $\varphi_\lambda^{(1)}$, $\varphi_\lambda^{(2)}$ and $\varphi_\lambda^{(3)}$:

$$\varphi_\lambda^{(1)} = x^l y^m z^n \mathbf{e}_i, \qquad 0 \leqq r < r_i, \tag{6a}$$

$$\varphi_\lambda^{(1)} = \frac{x^l y^m z^n r_i^k}{r^k} \mathbf{e}_i, \quad r_i \leqq r \leqq r_0, \tag{6b}$$

$$\varphi_\lambda^{(2)} = \frac{x^l y^m z^n r^j}{r_i^j} \mathbf{e}_i, \quad 0 \leqq r < r_i, \tag{7a}$$

$$\varphi_\lambda^{(2)} = \frac{x^l y^m z^n r_i^k}{r^k} \mathbf{e}_i, \quad r_i \leqq r \leqq r_0, \tag{7b}$$

and

$$\varphi_\lambda^{(3)} = x^l y^m z^n \mathbf{e}_i, \qquad 0 \leqq r \leqq r_0, \tag{8}$$

where displacement continuity at $r = r_i$ is realized by introducing r_i^k or r_i^j into equations (6b) and (7).

Assuming that $\varphi^{(1)}$ is the necessary base function in this system, we have three possible combinations among them; $\varphi^{(1)}$–$\varphi^{(2)}$, $\varphi^{(1)}$–$\varphi^{(3)}$, and $\varphi^{(1)}$–$\varphi^{(2)}$–$\varphi^{(3)}$. A preliminary assessment was conducted in the spherical co-ordinate. Although the $\varphi^{(1)}$–$\varphi^{(2)}$–$\varphi^{(3)}$ combination seems to be most effective, it was found to be too redundant to decrease internal independency among them, or to be more likely to fail in solving eigenvalue problem at lower N. $\varphi^{(1)}$–$\varphi^{(2)}$ and $\varphi^{(1)}$–$\varphi^{(3)}$ combinations usually provided a similar performance.

The configuration of extremely low acoustic impedance is of prime interest for developing the liquid–solid hybrid resonance experiments [6]. Therefore, I examined the case of $\rho_i/\rho_o = 0{\cdot}1$, $v_{pi}/v_{po} = 0{\cdot}1$, $v_{si}/v_{so} = 0{\cdot}1$ as an extreme case. As shown in Table 3, the $\varphi^{(1)}$–$\varphi^{(2)}$ combination yields much better results than those by the $\varphi^{(1)}$–$\varphi^{(3)}$ combination, for the case

TABLE 3

Comparison of performance between the two base function sets for a laminated sphere; $\rho_i/\rho_o = 0{\cdot}1$, $v_{pi}/\rho_{po} = 0{\cdot}1$, $v_{si}/s_{so} = 0{\cdot}1$, *and* $r_i/r_o = 0{\cdot}5$. *The numbers after the mode indices are the normalized analytical frequencies*

Mode index	$\varphi^{(1)}$–$\varphi^{(2)}$ base functions $N = 15$, $k = 8$, $j = 15$	$\varphi^{(1)}$–$\varphi^{(3)}$ base functions $N = 15$, $k = 7$
${}_0S_0$ (0·49493)	1·0000	1·0000
${}_0T_2$ (0·36680)	1·0000	1·0000
${}_0T_3$ (0·44477)	1·0000	1·0001
${}_1T_2$ (0·57878)	1·0000	1·0031

TABLE 4

Convergent frequencies and their partial derivatives for several typical modes in a laminated cylinder, whose height is equal to its diameter. Mode indices are an analogy of those of a sphere (Appendix B). The calculation conditions are $N = 15$, $k = 11$, $j = 17$; $N = 17$, $k = 11$, $j = 21$; $N = 19$, $k = 15$, $j = 21$; *the values of k and j are not as significant as N*

Mode index	Convergent frequency, f	$\dfrac{\partial \log f}{\partial \log v_{pi}}$	$\dfrac{\partial \log f}{\partial \log v_{si}}$	$\dfrac{\partial \log f}{\partial \log v_{po}}$	$\dfrac{\partial \log f}{\partial \log v_{so}}$
${}_0S_0$	0·27063	0·46	0·60	0·21e-3	0·86e-3
${}_1S_0$	0·34053	0·41	0·48	0·34e-1	0·74e-1
${}_1T_1$	0·24431	0	1·0	0	0·52e-3
${}_2T_1$	0·44675	0	1·0	0	0·55e-3

with large wave number w_{in} owing to relatively low acoustic velocities in the inner region. Therefore, the $\varphi^{(1)}$–$\varphi^{(2)}$ combination is the best recommended algorithm for a laminated system in the spherical co-ordinate.

Thus, the performance of the $\varphi^{(1)}$–$\varphi^{(2)}$ combination is examined as well in the cylindrical co-ordinate; the conditions except for shape are similar to those of Table 3. Although the gross convergency is worse than that in the spherical co-ordinate, some modes are confirmed to be convergent by $N = 15$. Table 4 shows convergent numerical frequencies, and its partial derivatives over velocities, for some typical modes free from angular dependency. Note that we have five digits of the same frequency over $N = 15$, 17, 19 for these modes. The convergent numerical frequencies of ${}_1T_1$ and ${}_2T_1$ are exactly the same as those analytical solutions. Among these modes, ${}_1T_1$ converges as fast as by $N = 7$, and ${}_0S_0$ and ${}_2T_1$ by $N = 11$. Besides the typical modes shown in Table 4, we have an additional 12 modes matching the present convergent criterion over $N = 15$, 17, 19. From the magnitude of partial derivatives, we can conclude that ${}_qS_0$ modes are most sensitive to v_{pi}, while ${}_qT_1$ modes are insensitive to v_{pi}. These modes are really important to constrain v_{pi} and v_{si} in the liquid–solid hybrid resonance technique, as reported in the preliminary work [6].

ACKNOWLEDGMENTS

The author thanks Drs N. Suda, M. Kumazawa, H. Kumagai, and K. Ishihara, at Nagoya University, for discussions. He is also grateful to Profs. I Suzuki, H. Oda, and

M. Walter, at Okayama University, and Prof. I. Ohno, at Ehime University, for helpful comments.

REFERENCES

1. W. H. VISSCHER, A. MIGLIORI, T. M. BELL and R. A. REINERT 1991 *Journal of the Acoustical Society of America* **90**, 2154–2162. On the normal modes of free vibration of inhomogeneous and anisotropic elastic objects.
2. R. HOLLAND 1968 *Journal of the Acoustical Society of America* **43**, 988–997. Resonant properties of piezoelectric deramic rectangular parallelepipeds.
3. H. H. DEMAREST JR 1971 *Journal of the Acoustical Society of America* **49**, 768–775. Cube-resonance method to determine the elastic constants of solids.
4. I. OHNO 1976 *Journal of Physics of the Earth* **24**, 355–379. Free vibration of a rectangular parallelepiped crystal and its application to determination of elastic constants of orthorhombic crystals.
5. M. SENOO and T. NISHIMURA 1984 *Bulletin of Japanese Society of Mechanical Engineers* **27**, 2339–2346. Measurement of elastic constants of polycrystals by the resonance method in a cylindrical specimen.
6. A. YONEDA 1998 *Reviews of High Pressure in Science and Technology* **7**, 79–82, Liquid–solid hybrid resonance method for investigating acoustic properties of magmas.

APPENDIX A: BRIEF REVIEW OF THE *xyz* ALGORITHM DEVELOPED BY VISSCHER *ET AL.*

In the *xyz* algorithm, the displacement in the *i*th direction $u_i(x, y, z)$ is expanded as

$$u_i = \sum a_{\lambda_i} \varphi_{\lambda_i}, \qquad \varphi_{\lambda_i} = x^l y^m z^n \mathbf{e}_i, \tag{A1, A2}$$

where $\mathbf{e}_i$ ($i = 1, 2, 3$) is a directional unit vector in the Cartesian co-ordinate. The integers l, m, and n are limited by an integer N as

$$l + m + n \leqslant N. \tag{A3}$$

The Lagrangian L is written as

$$L = \int \left(\frac{1}{2} \rho \omega^2 u_i u_i - \frac{1}{2} C_{ijkl} \frac{\partial u_i}{\partial x_j} \frac{\partial u_k}{\partial x_l} \right) \mathrm{d}V, \tag{A4}$$

where ρ is the density and ω the angular frequency. Substituting equation (A1) into equation (A4), we have

$$L = \tfrac{1}{2} (\omega^2 \mathbf{a}^{\mathrm{T}} E \mathbf{a} - \mathbf{a}^{\mathrm{T}} \Gamma \mathbf{a}), \tag{A5}$$

where the (λ_i, λ_k) component of the matrices E and Γ are given as

$$E_{\lambda_i \lambda_k} = \delta_{ik} \int \rho \varphi_{\lambda_i} \varphi_{\lambda_k} \mathrm{d}V, \qquad \Gamma_{\lambda_i \lambda_k} = \int C_{ijkl} \frac{\partial u_i}{\partial x_j} \frac{\partial u_k}{\partial x_l} \mathrm{d}V. \tag{A6, A7}$$

As we express the displacement as equation (A1), the variation of displacement is given by

$$\mathbf{a} \to \mathbf{a} + \delta \mathbf{a}. \tag{A8}$$

Thus, the variation of L is

$$\delta L = \tfrac{1}{2}(\mathbf{a}^{\mathrm{T}} + \delta\mathbf{a}^{\mathrm{T}})(\omega^2 E - \Gamma)(\mathbf{a} + \delta\mathbf{a}) - \tfrac{1}{2}\mathbf{a}^{\mathrm{T}}(\omega^2 E - \Gamma)\mathbf{a}$$

$$= \tfrac{1}{2}\mathbf{a}^{\mathrm{T}}(\omega^2 E - \Gamma)\delta\mathbf{a} + \tfrac{1}{2}\delta\mathbf{a}^{\mathrm{T}}(\omega^2 E - \Gamma)\mathbf{a}. \tag{A9}$$

Note that both E and Γ are asymmetric matrices, the stationary condition of $\delta L = 0$ is satisfied with

$$\omega^2 E\mathbf{a} = \Gamma\mathbf{a}. \tag{A10}$$

As E is not a diagonal matrix owing to the non-orthogonality of the present base functions, or power functions, equation (A10) is a generalized eigenvalue problem. Nowadays, we can solve equation (A10) on an ordinary workstation by means of a ready-made subroutine found in various numerical computation packages.

Note that the Legendre base functions provide us with a diagonal matrix of E owing to their orthogonality. Thus equation (A10) is simplified as an ordinary eigenvalue problem; it used to be critical to save memory and CPU time even on the most powerful computer 20–30 years ago.

APPENDIX B: GENERALIZED SOLUTIONS OF EIGENVIBRATION FOR A SPHERE AND A CYLINDER

Sphere:

Note that U corresponds to P-waves, and V and W are S-waves. The potential for P-waves is written as

$$\Phi = \mathrm{e}^{\mathrm{i}\omega t} P_n^m(\cos\theta)\frac{\mathrm{J}_{n+0\cdot5}(hr)}{\sqrt{r}}\mathrm{e}^{\mathrm{i}m\varphi}.$$

For S-waves, h should be replaced by k. Therefore, angular frequency is given as $\omega = v_p h = v_s k$ for h and k satisfying the boundary conditions

$$U_r = \frac{\partial\Phi}{\partial r}, \qquad U_\theta = \frac{\partial\Phi}{r\partial\theta}, \qquad U_\phi = \frac{\partial\Phi}{r\sin\theta\partial\phi},$$

$$V_r = 0, \qquad V_\theta = \frac{\partial\Phi}{\sin\theta\partial\phi}, \qquad V_\phi = -\frac{\partial\Phi}{\partial\theta},$$

$$W_r = -\frac{1}{r\sin\theta}\left\{\frac{\partial}{\partial\theta}\left(\sin\theta\frac{\partial\Phi}{\partial\theta}\right) + \frac{1}{\sin\theta}\frac{\partial^2\Phi}{\partial\phi^2}\right\},$$

$$W_\theta = \frac{\partial^2(r\Phi)}{r\partial r\partial\theta}, \qquad W_\phi = \frac{\partial^2(r\Phi)}{r\sin\theta\partial r\,\partial\theta},$$

$$U_r = \left(\frac{n\mathrm{J}_{0\cdot5+n}(hr) - hr\mathrm{J}_{1\cdot5+n}(hr)}{r^{1\cdot5}}\right)P_n^m(\cos\theta)\,\mathrm{e}^{\mathrm{i}m\phi}\mathrm{e}^{\mathrm{i}\omega t},$$

$$U_\theta = \frac{\mathrm{J}_{0\cdot5+n}(hr)}{r^{1\cdot5}} \frac{\{(n+1-m)P^m_{n+1}(\cos\theta) - (n+1)\cos\theta P^m_n(\cos\theta)\}}{\sin\theta} \mathrm{e}^{\mathrm{i}m\phi}\mathrm{e}^{\mathrm{i}\omega t},$$

$$U_\phi = \mathrm{i}\frac{m\mathrm{J}_{0\cdot5+n}(hr)}{r^{1\cdot5}} \frac{P^m_n(\cos\theta)}{\sin\theta} \mathrm{e}^{\mathrm{i}m\phi}\mathrm{e}^{\mathrm{i}\omega t},$$

$$V_r = 0,$$

$$V_\theta = \mathrm{i}\frac{m\mathrm{J}_{0\cdot5+n}(kr)}{r^{0\cdot5}} \frac{P^m_n(\cos\theta)}{\sin\theta} \mathrm{e}^{\mathrm{i}m\phi}\mathrm{e}^{\mathrm{i}\omega t},$$

$$V_\phi = \frac{\mathrm{J}_{0\cdot5+n}(kr)}{r^{0\cdot5}} \frac{\{(n+1-m)P^m_{n+1}(\cos\theta) - (n+1)\cos\theta P^m_n(\cos\theta)\}}{\sin\theta} \mathrm{e}^{\mathrm{i}m\phi}\mathrm{e}^{\mathrm{i}\omega t},$$

$$W_r = \frac{n(n+1)\mathrm{J}_{0\cdot5+n}(kr)}{r^{1\cdot5}} P^m_n(\cos\theta)\mathrm{e}^{\mathrm{i}m\phi}\mathrm{e}^{\mathrm{i}\omega t},$$

$$W_\theta = \frac{\{(n+1)\mathrm{J}_{0\cdot5+n}(kr) - kr\mathrm{J}_{1\cdot5+n}(kr)\}}{r^{1\cdot5}} \times \frac{\{(n+1-m)P^m_{n+1}(\cos\theta) - (n+1)\cos\theta P^m_n(\cos\theta)\}}{\sin\theta} \mathrm{e}^{\mathrm{i}m\phi}\mathrm{e}^{\mathrm{i}\omega t},$$

$$W_\phi = \mathrm{i}m\left\{\frac{(n+1)\mathrm{J}_{0\cdot5+n}(kr) - kr\mathrm{J}_{1\cdot5+n}(kr)}{r^{1\cdot5}}\right\} \frac{P^m_n(\cos\theta)}{\sin\theta} \mathrm{e}^{\mathrm{i}m\phi}\mathrm{e}^{\mathrm{i}\omega t}.$$

We can classify two types of vibration modes for an isotropic sphere as seismological notation for the earth's free oscillation. Vs have no radial component, and are called toroidal modes ${}_qT_n$. The combinations of Us and Ws have the radial component, and are called spheroidal modes ${}_qS_n$. The former subscript q is radial order corresponding to the number of nodal surfaces inside the sphere, while the latter angular order corresponds to the number of nodal lines on the spherical surface. Note that the number of nodal lines on the surface is n for ${}_qS_n$ modes and $n-1$ for ${}_qT_n$ modes.

Note that there are two types of Bessel functions; the first kind Bessel function $\mathrm{J}(r)$ is finite at $r=0$, while the second kind of $\mathrm{Y}(r)$ is infinite at $r=0$. Thus the above expression, written with the first kind of Bessel function, J, is only valid for a solid sphere, which comprises $r=0$ in the system. On the other hand, the second kind Bessel function, Y, must be introduced for a bored sphere or a shell, because it is free from the infinity at $r=0$. Thus, J_n should be replaced with $A\mathrm{J}_n + B\mathrm{Y}_n$, such as

$$U_\phi = \mathrm{i}\frac{m(A\mathrm{J}_{0\cdot5+n}(hr) + B\mathrm{Y}_{0\cdot5+n}(hr))}{r^{1\cdot5}} \frac{P^m_n(\cos\theta)}{\sin\theta} \mathrm{e}^{\mathrm{i}m\phi}\mathrm{e}^{\mathrm{i}\omega t},$$

where A and B are constants adjusted to satisfy the inner and the outer boundary conditions. The situation is the same in the cylindrical co-ordinate as well.

Cylinder:

The notations are similar as in the case of the spherical co-ordinate. However, the potential is given as

$$\Phi = \mathrm{e}^{\mathrm{i}\omega t}\,\mathrm{J}_m(hr)\mathrm{e}^{\mathrm{i}nz}\mathrm{e}^{\mathrm{i}m\theta}.$$

The angular frequency is given as $\omega = v_p\sqrt{h^2+n^2} = v_s\sqrt{k^2+n^2}$ for h, k and n satisfying the boundary conditions. Although the following solutions are written for J, it should be replaced with $A\mathrm{J} + B\mathrm{Y}$ in the case of a tube, as discussed in the spherical co-ordinate:

$$U_r = \frac{\partial \Phi}{\partial r}, \qquad U_\theta = \frac{\partial \Phi}{r\partial\theta}, \qquad U_z = \frac{\partial \Phi}{\partial z},$$

$$V_r = \frac{\partial \Phi}{r\partial\theta}, \qquad V_\theta = -\frac{\partial \Phi}{\partial r}, \qquad V_z = 0,$$

$$W_r = \frac{\partial^2 \Phi}{\partial r\partial z}, \qquad W_\theta = \frac{\partial^2 \Phi}{r\partial\theta\partial z}, \qquad W_z = -\left\{\frac{\partial^2\Phi}{\partial r^2} + \frac{\partial\Phi}{r\partial r} + \frac{\partial^2\Phi}{r^2\partial^2\theta}\right\},$$

$$U_r = \left(\frac{m\mathrm{J}_m(hr) - hr\mathrm{J}_{m+1}(hr)}{r}\right)\mathrm{e}^{\mathrm{i}m\theta}\mathrm{e}^{\mathrm{i}nz}\mathrm{e}^{\mathrm{i}\omega t}, \qquad U_\theta = \frac{m\mathrm{J}_m(hr)}{r}(\mathrm{i}\mathrm{e}^{\mathrm{i}m\theta})\mathrm{e}^{\mathrm{i}nz}\mathrm{e}^{\mathrm{i}\omega t},$$

$$U_z = n\mathrm{J}_m(hr)\,\mathrm{e}^{\mathrm{i}m\theta}(\mathrm{i}\mathrm{e}^{\mathrm{i}nz})\mathrm{e}^{\mathrm{i}\omega t}, \qquad V_r = \frac{m\mathrm{J}_m(kr)}{r}(\mathrm{i}\mathrm{e}^{\mathrm{i}m\theta})\mathrm{e}^{\mathrm{i}nz}\mathrm{e}^{\mathrm{i}\omega t},$$

$$V_\theta = -\left(\frac{m\mathrm{J}_m(kr) - kr\mathrm{J}_{m+1}(kr)}{r}\right)\mathrm{e}^{\mathrm{i}m\theta}\mathrm{e}^{\mathrm{i}nz}\mathrm{e}^{\mathrm{i}\omega t}, \qquad V_z = 0,$$

$$W_r = n\left(\frac{m\mathrm{J}_m(kr) - kr\mathrm{J}_{m+1}(kr)}{r}\right)\mathrm{e}^{\mathrm{i}m\theta}\mathrm{e}^{\mathrm{i}nz}\mathrm{e}^{\mathrm{i}\omega t}, \qquad W_\theta = \frac{mn\mathrm{J}_m(kr)}{r}(\mathrm{i}\mathrm{e}^{\mathrm{i}m\theta})\mathrm{e}^{\mathrm{i}nz}\mathrm{e}^{\mathrm{i}\omega t},$$

$$W_z = k^2\mathrm{J}_m(kr)\,\mathrm{e}^{\mathrm{i}m\theta}(\mathrm{i}\mathrm{e}^{\mathrm{i}nz})\mathrm{e}^{\mathrm{i}\omega t}.$$